Cerebral Cortex, June 2018;28: 2085–2099

doi: 10.1093/cercor/bhx114
Advance Access Publication Date: 4 May 2017
Original Article

ORIGINAL ARTICLE

Functional Similarity of Medial Superior Parietal Areas for Shift-Selective Attention Signals in Humans and Monkeys

Natalie Caspari[1,2], John T. Arsenault[1,3], Rik Vandenberghe[2,4] and Wim Vanduffel[1,3,5]

[1]Laboratory for Neuro- and Psychophysiology, Department of Neurosciences, KU Leuven Medical School, 3000 Leuven, Belgium, [2]Laboratory for Cognitive Neurology, Department of Neurosciences, KU Leuven, 3000 Leuven, Belgium, [3]Massachusetts General Hospital, Martinos Center for Biomedical Imaging, Charlestown, MA 02129, USA, [4]University Hospitals Leuven, Department of Neurology, 3000 Leuven, Belgium and [5]Harvard Medical School, Department of Radiology, Boston, MA 02115, USA

Address correspondence to Wim Vanduffel, KU Leuven, Laboratory for Neuro- and Psychophysiology, Campus Gasthuisberg, O&N 2, Herestraat 49-bus 1021, 3000 Leuven, Belgium. Email: wim@nmr.mgh.harvard.edu

Abstract

We continually shift our attention between items in the visual environment. These attention shifts are usually based on task relevance (top-down) or the saliency of a sudden, unexpected stimulus (bottom-up), and are typically followed by goal-directed actions. It could be argued that any species that can covertly shift its focus of attention will rely on similar, evolutionarily conserved neural substrates for processing such shift-signals. To address this possibility, we performed comparative fMRI experiments in humans and monkeys, combining traditional, and novel, data-driven analytical approaches. Specifically, we examined correspondences between monkey and human brain areas activated during covert attention shifts. When "shift" events were compared with "stay" events, the medial (superior) parietal lobe (mSPL) and inferior parietal lobes showed similar shift sensitivities across species, whereas frontal activations were stronger in monkeys. To identify, in a data-driven manner, monkey regions that corresponded with human shift-selective SPL, we used a novel interspecies beta-correlation strategy whereby task-related beta-values were correlated across voxels or regions-of-interest in the 2 species. Monkey medial parietal areas V6/V6A most consistently correlated with shift-selective human mSPL. Our results indicate that both species recruit corresponding, evolutionarily conserved regions within the medial superior parietal lobe for shifting spatial attention.

Key words: fMRI, homology, macaque, selective attention, spatial shifting

Introduction

To dynamically select behaviorally relevant objects in the visual scene, we continually alternate short intervals of sustained attention with rapid shifts in attention to specific locations or objects. These rapid shifts in attention are typically followed by eye, head, and hand movements to guide goal-directed behavior.

Transient shifts of spatial attention activate the human medial superior parietal lobe (mSPL), producing signals independent of the direction of the attention shift (Vandenberghe et al. 2001; Yantis et al. 2002; Molenberghs et al. 2007; Kelley et al. 2008).

Aside from functional studies in healthy humans, causal evidence for SPL playing a critical role in spatial shifting comes

from a recent lesion study where a lesion of the medial wall of SPL resulted in a pathological increase in the invalidity effect for both left- and right-sided targets during a classical spatial cueing paradigm (Vandenberghe et al. 2012). Furthermore, Balint's syndrome (Bálint 1909), caused by lesions in occipito-parietal cortex including mSPL, is characterized by ocular apraxia, a deficit in generating purposeful voluntary eye movements, and simultagnosia, the inability to perceive more than one object at a time (Ptak and Müri 2013). Potentially, a common explanation for these deficits is a breakdown of attention shifts, independent of the direction of the shift (Vandenberghe et al. 2001, 2012). A compelling repetitive TMS study also revealed a double-dissociation whereby inactivation of the right ventral IPS impaired sustained attention processes while targeting mSPL affected target discrimination after a shift of attention (Capotosto et al. 2013).

While evidence for transient shift-selectivity of human mSPL is compelling, there is still doubt about the exact homology of this area in nonhuman primates. Recently, we identified several regions in occipito-parietal and frontal cortex of the monkey that were selectively activated by attention shifts (Caspari et al. 2015), whereas human spatial-attention shifts most strongly activated mSPL (Vandenberghe et al. 2001; Yantis et al. 2002; Molenberghs et al. 2007; Kelley et al. 2008). Hence, it is unclear which of these shift-selective regions observed in the monkey might correspond to human shift-selective mSPL, and whether potential differences in the activations might have occurred due to the different task designs of previous human studies.

Therefore, the goal of the present study was to determine, in a data-driven manner, whether the shift-selective human mSPL is functionally homologous to the medial parietal or frontal shift-selective foci in monkeys, using identical experimental paradigms in both species. To this end, we performed a selective spatial-attention task in 31 human subjects that was based on the experiments by Molenberghs et al. (2007), although slightly adapted to match more closely the paradigm applied to monkeys by Caspari et al. (2015). Periods of sustained attention ("stay events") were interleaved with shifts of attention ("shift events"). Critically, we dissociated the actual attention shifts from the motor and visual events used to behaviorally track the subject's allocation of attention. Furthermore, in supplementing traditional parametric fMRI analyses, we introduced a novel data-driven comparative method that is devoid of spatial assumptions. This is achieved by correlating the task event-related beta-values, obtained from the shift-selective attention region in human mSPL, to the corresponding beta-values of each voxel in monkeys (interspecies beta-correlation [ISBC]). This analytical method is inspired by the interspecies activity correlation (ISAC) method (Mantini et al. 2012) in which fMRI timecourses are correlated across species, but with the additional advantage that ISBC does not require exactly matched task events in the temporal domain. Since ISBC considers all modeled conditions, rather than just a few ones used in a GLM-based contrast, this new method provides a much richer view on the shared functional properties of putative homologous areas. In fact, the more conditions modeled in a given experiment, the better this correlational method should perform, unlike cross-species comparisons based on standard GLM-based methods. Interestingly, the ISBC approach is reminiscent of the fingerprint matching approach based on patterns of correlation in brain activity across species as measured with resting state fMRI (Neubert et al. 2015).

We show that voxels in monkey medial and lateral parietal and in frontal cortex correlated with those of the human mSPL-cluster, when all conditions modeled by the GLM (and not just those selected for the computation of a specific contrast) were considered. When focusing onto the most strongly shift-selective voxels of mSPL, significantly correlated ROIs were confined mainly to monkey medial occipito-parietal cortex. Our results underscore the view that spatial attention shifts are computed by the medial superior parietal lobule in both humans and monkeys.

Materials and Methods

Subjects

Human

Thirty-two volunteers (mean age 25 years, range 20–32 years, 12 male) participated in the experiment. All participants were right-handed, had normal or corrected-to-normal visual acuity and no history of mental illness or neurological diseases. The study was approved by the Ethical Committee of the KU Leuven Medical School and all volunteers gave their written informed consent in accordance with the Helsinki Declaration prior to the experiment. One subject (male) was excluded from the analysis, because of fatigue and decreased performance during the experiment. The present data are based on the remaining 31 subjects.

Monkey

Three rhesus monkeys, including 2 females (M13, M24, and M35; Macaca mulatta; 3–6 kg; 3–9 years of age) participated in the experiments. Animal care and experimental procedures were performed in accordance with the National Institute of Health's "Guide for the Care and Use of Laboratory Animal", the European legislation (Directive 2010/63/EU) and were approved by the Ethical Committee at the KU Leuven. Animal housing and handling were in accordance with the recommendations of the Weatherall report, allowing locomotor behavior, social interactions, and foraging. Animals were pair- or group-housed (2–5 animals per group; cage size at least 16–32 m^3) with cage enrichment (toys and foraging devices), outside views and natural day-night cycles at the primate facility of the KU Leuven Medical School. They were daily fed with standard primate chow supplemented with bread, nuts, raisins, prunes, and fruits. The animals received their water supply either during the experiments, or in the cages before and after the experiments. The details of the general fMRI procedures and training of monkeys have been described previously (Vanduffel et al. 2001; Nelissen et al. 2005; Caspari et al. 2015).

Stimuli and Tasks

Spatial Shift Experiment

For the human subjects, the experimental paradigm of Molenberghs et al. (2007) was adapted to match the monkey experiment (Caspari et al. 2015) as closely as possible. The monkey data of the Caspari et al. (2015) study is used in this manuscript. Two stimuli were placed on the horizontal meridian at 9.25 deg eccentricity, in the left and right hemifields (Fig. 1, panel I). All stimuli were white on a black background and of equal area (1.59 deg^2). There were 2 possible coupled stimulus pairs, a square with a triangle and a circle with a diamond. Each pair contained a relevant and an irrelevant stimulus. Relevant stimuli remained fixed for each subject, and were counterbalanced across human and monkey subjects. They were identical for M13 and M35 (square and circle), and swapped for M24 (triangle and diamond).

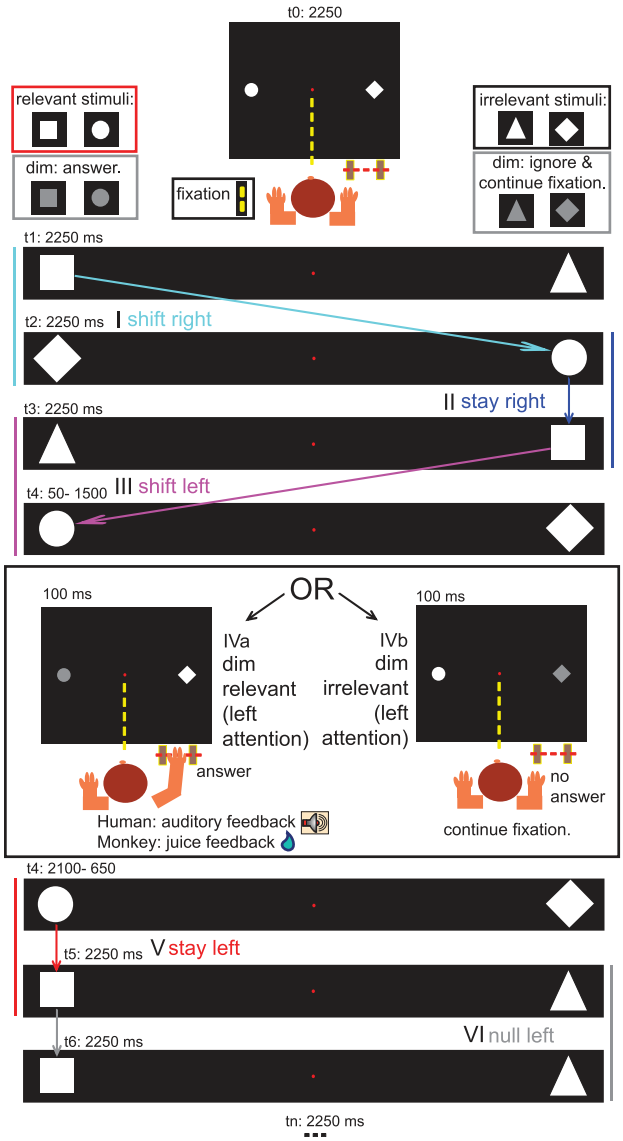

Figure 1. Stimuli and Task. Top (schematic of display viewed by the subject): Subjects fixated centrally during all trial types, and also when responding to dimming events. One stimulus pair (consisting of a relevant and irrelevant shape) was presented every time that subjects performed the task correctly. Each pair was replaced, without temporal gap, by the succeeding pair after 2250 ms. Top left: Dimming of the relevant shapes had to be indicated by a manual response (both humans and monkeys) followed by auditory feedback (humans), or by feedback as a juice reward (monkeys). Top right: Dimming of the irrelevant shapes had to be ignored. Examples of different event types I) shift right: a feature-change cues the subject to covertly shift attention to the right hemifield (the left relevant stimulus (square) is replaced by an irrelevant one (diamond)); II) stay right: a feature-change cues the subject to maintain his covert attention to the right, since the relevant stimulus (square) of the next pair appears at the same position as the preceding one (circle); III) shift left; IVa) dim relevant, left attention: upon a relevant dimming, the subject responds and receives either an auditory feedback tone (humans) or a liquid reward (monkeys); IVb) dim irrelevant, left attention: irrelevant dimming in the hemifield contralateral to the attended relevant stimulus, the subject continues fixating, no feedback is given; V) stay left; VI) null left: same shapes remain at the same position for 2 × 2250 ms.

To perform the task correctly, subjects had to respond by manually interrupting a light beam when the relevant (Fig. 1, panel IVa), but not the irrelevant, stimulus dimmed (Fig. 1, panel IVb). Subjects were trained to covertly attend the relevant stimulus of each pair, and to fixate upon the central fixation point during the entire task while eye and hand positions were monitored. They covertly maintained attentional focus at the location of the relevant stimuli, which was probed with occasional randomly inserted dimming events (the relevant and irrelevant shapes dimmed for 100 ms in 14% of the trials each). Luminance contrast (gray level) was adapted on a run-wise basis to approximate a performance level of 85% uninterrupted, correctly performed trials, to avoid ceiling levels in behavioral performance.

The sustained attention baseline was transiently interrupted by 2 types of events. These consisted of a replacement (without temporal gaps) of one stimulus pair by the second stimulus pair, occupying the same positions. In the first event type (Fig. 1, panels I & III), the relevant stimulus of the new pair appeared at the position previously occupied by the irrelevant stimulus of the preceding pair, and vice versa. This feature change, in combination with a positional change of the relevant stimulus, elicited a shift in spatial attention (shift event). A "shift-right" event (Fig. 1, panel I) corresponded to a spatial shift of the relevant stimulus from the left to the right hemifield, and a "shift-left" (Fig. 1, panel III) to a spatial shift from right to left. In event type 2 (Fig. 1, panels II & V), the relevant stimulus of the new pair appeared at the same position as the relevant stimulus of the preceding pair. Hence, the relevant stimulus site remained unchanged, inducing no spatial shift in attention. This was called a "stay" event ("stay-right" [Fig. 1, panel II], or "stay-left" [Fig. 1, panel V]). With this event, attention was already deployed at the target location before the feature change (= event onset). One-third of the trials were "null" events (Fig. 1, panel VI, "null left"). During these events, the stimuli remained on the screen without being changed. Each run contained an equal number of shift, stay, and null events. The positions occupied by the stimuli, as well as the number of relevant and irrelevant dimming events, were matched across event types. Dimmings were equally distributed between 50 and 1500 ms after event onset.

Human subjects fixated on a red dot (0.3 deg) inside an approximately 4 × 5 deg fixation window (depending on the quality of the eye data) during the consecutive stimulus displays. Meanwhile they kept their thumbs passively positioned in the infrared light beam on the response key. During the relevant dimmings, short thumb movements (unblocking the light beam) were used as operant behavior. Correct answers after the dimming were followed by an auditory feedback beep tone, to mimic the feedback-function of the liquid reward in monkeys. Furthermore, subjects received a per-run additional monetary bonus when they detected 75% of the dimmings per run. They were informed about the bonus after each run. Moving the thumb when no relevant dimming occurred resulted in an abort of the stimulus display (false alarm, similarly to the monkey experiment). Half of the subjects responded with the left thumb, the other half with the right thumb.

Monkey subjects were trained to fixate on a red dot (0.3 deg) inside a 2 × 3 deg fixation window during the continuous stimulus displays, while keeping their hands in the response box. Correct answers after the relevant dimmings were followed by a liquid reward feedback. Fixation-only trials were not rewarded. The position of both hands within the response box during the trial sequence was checked using infrared light beams. This procedure minimized unwanted (hand) movements, or saccadic eye movements toward the peripheral stimuli. In cases where the monkeys made a hand movement

(except during the dimming of the relevant stimulus) or an eye movement outside the fixation window, the trial was aborted and the stimulus display disappeared (Caspari et al. 2015). M13 and M24 responded in 50% of the scan sessions with the right hand and the other half with the left hand. Since the data of interest in these 2 monkeys did not change as function of the hand used, M35 was trained to respond with the left hand only.

Functional MRI Acquisition

Procedure

Human subjects received 1 h of training prior the experiment, for fixation and for responding during the event-related behavioral task, while eye and hand positions were monitored. This session also served to determine the luminance contrast (gray level) for the dimmings that resulted in a detection rate of 80–85% for each individual subject. The stimuli were projected with a liquid crystal display projector (PA500U; 1920 × 1200, 60 Hz refresh frequency; NEC) onto a translucent screen positioned in the back of the bore of the magnet, 70 cm from the eyes. Participants viewed the stimuli through a mirror tilted 45° that was attached to the head coil. Eye positions were tracked through pupil position and corneal reflection (250 Hz, EyeLink1000). Each subject participated in one scanning session including 6 runs of the behavioral event-related task.

Monkeys were trained in a mockup of an MRI scanner for all tasks. They were scanned following several months (~4) of training, when fixation performance exceeded 90–95%, and when false-alarm rates approached zero percent. The monkey sat in a sphinx position, head fixed to the plastic monkey chair, directly facing the screen. Eye positions were monitored at 120 Hz, using pupil position and corneal reflection (Iscan).

Human MRI

Subjects were scanned with a 3.0 tesla horizontal bore full-body scanner (Philips Achieva d-stream system) equipped with a 32 channel iRF head coil, located at the University Hospital of KU Leuven. For all functional scans (except for the resting state scan), images of the whole brain were acquired using gradient-echo planar imaging with the following parameters: 36 transverse slices (2.75 × 2.75 × 3.5 mm voxel size; 0.25 mm gap), repetition time (TR), 2 s; time of echo (TE), 30 ms; flip angle, 90°; 80 × 87 matrix with 2.7 × 2.7 mm in-plane resolution, and SENSE reduction factor of 2. The resting state functional scans were acquired with 31 slices (3.59 × 3.59 × 4.0 mm voxel size; 0 mm gap); TR, 1750 ms; TE, 33 ms; flip angle, 90°; 64 × 64 matrix with 3.59 × 3.59 mm in plane resolution, and SENSE reduction factor of 2.

A 3-dimensional, high resolution T1-weighted image (0.89 × 0.89 × 1 mm voxel size) covering the entire brain was acquired in the same session and used for anatomical reference (TE/TR, 9.7/4.6 ms; inversion time, 900 ms; slice thickness, 1 mm; 256 × 256 matrix; 208 coronal slices; SENSE reduction factor, 2).

The main experiment (spatial shifting task) was scanned using an event-related design, with each run lasting 500 s (250 volumes, including 4 dummy volumes). The resting state scan lasted 600 s (343 volumes, including 4 dummy scans).

Monkey MRI

Using a gradient-echo T2*-weighted echo-planar imaging-sequence, we acquired data for the (1) selective attention task (40 horizontal slices; TR, 2 s; TE, 17 ms (M13, M24), 19 ms (M35); 1.25 × 1.25 × 1.25 mm^3 isotropic voxels, image acceleration factor of 3 (M13, M24), or 2 (M35)) and for the (2) resting state scans used for the functional connectivity analyses (36 horizontal slices; TR of 1.4 s; TE, 16 ms; 1.25 × 1.25 × 1.25 mm^3 isotropic voxels, image acceleration factor of 3 (M13, M24), or 2 (M35). M13 was scanned with a custom-built, 8-channel phased-array receiver coil, and a saddle-shaped, radial transmit-only surface coil (Kolster et al. 2009). M24 and M35 had been implanted with 8- and 5-channel receiver coil arrays, respectively, mounted on top of the skull, beneath the headpost, improving sensitivity for MR-imaging (Janssens et al. 2012). Scanning of M24 was performed with the same scanner, main parameters, and transmit coil as with M13, but with the addition of a 36 cm inner-diameter head gradient set (AC88, maximum strength: 80 mT/m; maximum slew rate: 800 T/m/s). The resting-state scans of M35 were also performed with the AC88 (in order to reach the same parameters as for M13/M24 with the 5-channel implant coils). Slices were oriented transversally, covering the entire brain. As MION (Sinerem; Laboratoire Guerbet, or Feraheme) measurements depended only on blood volume (Mandeville and Marota 1999), all signal values have been inverted.

The main selective-attention task was scanned using an event-related design, and a run lasted 610 s (305 volumes, including 4 dummy volumes). The resting-state scans were acquired at a different date after the selective attention experiment, subjects were awake while fixating, with runs lasting 590.8 s (422 volumes, including 4 dummy volumes).

High-resolution anatomical images were acquired for each monkey in separate scan sessions under anesthesia, using a single radial transmit-receive surface coil and an MPRAGE sequence (TR, 2200 ms; TE, 4.05 ms; 208 slices; 0.4 mm isotropic voxel size).

fMRI Data Analysis

Preprocessing of the Human Data

Data analysis was performed using the SPM8 software package (Wellcome Department of Cognitive Neurology) running under MATLAB (The Mathworks, Inc.). The preprocessing steps involved the following: (1) realignment of the images, (2) slice time correction (3) coregistration of the anatomical image and the mean functional image, and (4) segmentation of the anatomies and spatial normalization of all images to a standard stereotaxic space (Montreal Neurological Institute) with a voxel size of 3 × 3 × 3 mm. Resting state data were linearly detrended. Before further analysis, the functional data were smoothed with an isotropic Gaussian kernel of 5 × 5 × 7 mm.

Preprocessing of the Monkey Data

The raw EPI images were corrected for the lowest-order off-resonance effects and aligned with respect to the GRE reference images before performing a SENSE image reconstruction (Pruessmann et al. 1999). Residual N/2 artifacts in the reconstructed images were removed using an algorithm based on the UNFOLD method (Madore et al. 1999) and were further corrected for higher order distortions using a nonrigid slice-by-slice distortion correction (Kolster et al. 2009). Subsequent data analysis was performed using SPM5 software package (Wellcome Department of Cognitive Neurology) running under MATLAB (The Mathworks, Inc.). The preprocessing steps included (1) skull-stripping the images, (2) coregistration of the anatomical and mean functional images, and (3) spatial normalization of all images to the 112-RM atlas (McLaren et al. 2009) aligned to the F99 surface-based atlas (Van Essen et al. 2001), with a voxel size of 1 × 1 × 1 mm. Images were smoothed with a 1.5 mm kernel.

General Linear Model

As illustrated in Fig. 1 (and described above), the following events entered the GLM: stay events, composed of a feature change (Fig. 1 panel II: stay-right, Fig. 1 panel V: stay-left); shift events, composed of a feature change and a spatial shift (Fig. 1 panel I: shift-right, Fig. 1 panel III: shift-left); relevant dimming events (Fig. 1 panel IVa: dim answer left attention; dim answer right attention, not shown in Fig. 1); irrelevant dimming events (Fig. 1 panel IVb: dim no-answer left attention; dim no-answer right attention, not shown in Fig. 1); and null events, composed of no visual change of the stimuli (Fig. 1 panel VI: null left; and null right, not shown in Fig. 1). The number of correctly executed trials analyzed for each event type was equalized for left- and right-sided attention. Only trial sequences with at least 3 or more consecutive and correctly executed fixation trials were included in the analysis. The GLM thus included 10 regressors for the 10 conditions (1 – null left, 2 – null right, 3 – stay left, 4 – stay right, 5 – shift left, 6 – shift right, 7 – dim answer left attention, 8 – dim answer right attention, 9 – dim no answer left attention, 10 – dim no answer right attention) and 6 additional head motion regressors (translation and rotation in 3D) per run. In monkeys, 2 additional eye-movement regressors were included. Activations correlating with "transient" spatial attention shifts, irrespective of the direction of the shift, were visualized by contrasting bilateral "shifts" (shift and feature change) versus "stay" (feature change) events: 6- shift left and 7- shift right versus 3- stay left and 4- stay right.

For every human participant, the onset and duration of each condition was modeled using a GLM and all regressors were convolved with the canonical hemodynamic response function (HRF). Data were first analyzed per subject and scanning day (= session) with a fixed-effects general linear model (GLM). A second-level random effects analysis (RFX) was then performed on the contrast obtained from the first-level analyses (Holmes and Friston 1998).

For the monkey data, each condition was modeled by convolving a gamma function (delta = 0, tau = 8, and exponent = 0.3), modeling the MION HRF, at the onset of the condition (transition of stimulus displays). Data were first analyzed per subject and scanning day (= session) with a fixed-effects GLM. Runs with a fixation performance under 85% were excluded. For M13, this resulted in 8 sessions with a total of 119 runs (on average 14 runs/session), for M24, 12 sessions with a total of 181 runs (averaging 15 runs/session), and for M35, 10 sessions with a total of 171 runs (averaging 17 runs/session) that were included in the analyses. Next, we computed a session-wise second-level mixed-effect analysis (MFX; Friston et al. 2005; Caspari et al. 2015), with the "con-images" of the main contrast of interest, obtained from the first-level analyses, as input, including a total of 30 images per contrast (8 (M13) + 12 (M24) + 10 (M35) sessions).

Unless otherwise mentioned, statistical maps were thresholded at $P = 0.001$ (uncorrected) and a cluster extent threshold of 10 voxels was applied to all volume maps. The uncorrected threshold for the shifting contrast was motivated by the fact that we had a clear *a priori* hypothesis advocating superior parietal involvement (Molenberghs et al. 2007; Caspari et al. 2015).

Interspecies Beta-Correlation

Our intent was to characterize interregional correlations during distinct stages of our selective attention task, independently of the temporal occurrence of these stages within each species. We therefore employed the above-described GLM to estimate the stage-specific activity in each species for each of our 10 condition types, represented as a beta value for each condition and each voxel (Rissman et al. 2004). This set of parameter estimates (beta values) for each voxel reflects how much the voxel's activity can be attributed to each specific condition. These "beta-fingerprints" were then sorted per condition, yielding 10 beta estimates for each voxel (1 – null left, 2 – null right, 3 – stay left, 4 – stay right, 5 – shift left, 6 – shift right, 7 – dim answer left attention, 8 – dim answer right attention, 9 – dim no answer left attention, 10 – dim no answer right attention). Subsequently, averaging was done for each human subject ($n = 31$) separately, and for each monkey session ($n = 30$), each in its respective normalized group space.

ISBC of the Human Medial Shift-Selective SPL-Cluster with Voxels in Monkey (Statistics Across Monkey Sessions)

We first asked which voxels of the monkey brain correlated with the beta-fingerprints of the human shift-selective medial SPL-region, as it is typically defined (Vandenberghe et al. 2001; Yantis et al. 2002; Molenberghs et al. 2007). For this purpose, we averaged beta-fingerprints across the 31 human subjects within the entire medial SPL-cluster-ROI as defined by the GLM analysis contrasting shift versus stay conditions ($P < 0.005$) (Caspari et al. 2015). The average human SPL beta-fingerprints (represented by a beta value for each condition) were then used to compute the correlation with the voxel-wise beta-fingerprints of each individual monkey session acquired across the 3 animals, yielding 30 correlation maps. Correlation analyses were conducted using Matlab R2012b (http://www.mathworks.com). To allow for further statistical analysis, the 30 monkey correlation maps were then converted into z-scores according to Fisher's *r*-to-*z* transformation (Zar 1996). To assess the significance of the correlations at the group level, the z-transformed correlation maps of the individual monkey sessions were subjected to a group-level mixed-effects analysis and thresholded at $P = 0.05$ FWE corrected level in the volume (applying cluster extent threshold of 10 voxels), and at $P < 0.0001$ uncorrected ($t = 4.25$) for display on the gray matter surface.

ISBC of Monkey ROIs with Subregions of Human SPL (Statistics Across Human Subjects)

Secondly, we attempted to compute the pairwise beta-fingerprint correlations across anatomically (Eickhoff et al. 2005; Scheperjans et al. 2008) and functionally defined (present study) human SPL and independently defined monkey ROIs. For this analysis, the average beta-fingerprints (representing the 10 conditions) of each monkey region of interest (ROI, as listed in Supplementary Table 6) were correlated with the average beta-fingerprints of each human ROI in a subject-wise manner. To obtain the correlations between the ROI pairs displayed in the correlation matrix, the same averaging was performed as above (using Fisher's *r*-to-*z* transformation), but this time across human subjects per ROI-pair. Significances were computed based on the random-effects statistics across human subjects, and the resulting correlation matrices were Bonferroni-corrected (98 monkey ROIs × 3 human SPL-ROIs) for the number of comparisons indicated at $^{*}P < 0.05$, and $^{**}P < 0.01$.

ROI Definition in Human Subjects

The anatomical labels used for a number of human visual areas (V1–V3, V3A, V4, MT, and LOC) originated from the PALS-B12 atlas, as provided in FreeSurfer. SPL5 and SPL7 (Scheperjans et al. 2008),

PGa, PFm, and area PF (Caspers et al. 2006) and labels of anatomical locations were obtained from the SPM8 anatomy toolbox (Eickhoff et al. 2005). The SPL-regions comprised cytoarchitectonically defined areas 5L, 5M, and 5Ci (SPL5), and 7A, 7PC, 7M, and 7P (SPL7), respectively (Scheperjans et al. 2008). Three-millimeter spheres around the 4 highest local maxima of the medial SPL cluster (as listed in Supplementary Table 3, surviving FWE correction and non-overlapping), were used to represent the maximally shift-selective region within the medial SPL cluster (termed "SPLmx") as defined by the GLM-contrast shift versus stay. Areas PHC-2 and FEF in the volume sections of the seed-maps were localized by using the probabilistic ROIs of Arcaro et al. (2009) and Wang et al. (2005), respectively.

ROI Definition in Monkey

ROI outlines are displayed in Supplementary Fig. 1 on the inflated F99 gray matter surface, and ROI origins are listed in Supplementary Table 6. ROIs that entered the correlation analysis were mapped back from the surface to the volume to fill the gray matter ribbon in the volume-space of the segmented F99 group template using FreeSurfer (http://surfer.nmr.mgh.harvard.edu). Areal labels for V1, V2, V3, V4, V4A, PITd, PITv, areas MT, MSTv, and FST were derived from previous retinotopy experiments. These labels were defined based upon combined retinotopic labels over 5 monkeys (probability maps of 50% overlap, including M13 and M24) (Janssens et al. 2014; Caspari et al. 2015). Further labels in F99 space were derived from Lewis and Van Essen (2000a, 2000b) atlas and Ferry et al. (2000), Fattori et al. (2009), and Mantini et al. (2011). Labels from Nelissen et al. (2011) had previously been anatomically defined on the template anatomy of M12 (Ekstrom et al. 2009), and were warped to the F99 surface using the FreeSurfer surface-to-surface registration algorithm.

Surface-Based Projections

Flat maps were created performing the segmentation using FreeSurfer (http://surfer.nmr.mgh.harvard.edu/). All surface-maps were thresholded at a minimal surface area extent of 30 mm^2 (http://surfer.nmr.mgh.harvard.edu/fswiki/mri_surfcluster). For visualization, the resulting monkey statistical *t*-maps from the MFX analyses were projected onto the macaque F99 brain (Van Essen 2004), whereas the human statistical *t*-maps were projected onto the FreeSurfer fsaverage brain (MNI305), respectively, displayed as a flat map or an inflated view. For both species, projections onto the flatmaps (gray matter surface) were displayed at a slightly more lenient threshold of $P = 0.005$ (uncorrected) than that for the volumes.

Analysis of Behavioral Data

Behavioral data were obtained from at least 3 consecutively correctly executed trials. Monkey behavioral data were analyzed in a session-wise manner (for each subject), whereas human data were analyzed across subjects.

Probing the Allocation of Attention: Dimming of the Relevant Stimulus

Percent hits (detected relevant dimmings) and misses (undetected relevant dimmings) were calculated with respect to the overall number of response trials (relevant dimmings). False alarms (responses to irrelevant dimmings) were calculated relative to the total number of irrelevant dimmings. Reaction times (RTs) were analyzed to assess whether (1) subjects reacted equally fast after dimmings of relevant stimuli in the left or right visual hemifield and whether (2) differences in RTs existed between the relevant dimmings occurring right after one of the 3 trial types (null, stay, and shift). RTs were sampled for all correctly performed response trials during which a dimming of the relevant stimulus occurred no more than 600 ms after trial onset. Across-subject repeated-measures ANOVAs were performed with factors "condition" (null, stay, and shift) and "direction of attention" (left, right), for RTs, hits, and misses (Supplementary Table 1, human data; Supplementary Table 2, monkey data).

Eye-movement data during fixation-only trials

Eye-position data were analyzed for the fixation trials (correct sequences of at least 3 consecutive trials, excluding dimmings or rewards). This analysis was intended to track the eye position for correctly performed stimulus sequences within a specific fixation window (4 × 5 degrees of visual angle for humans, and 2 × 3 degrees for monkeys), with respect to each condition (see Supplementary Figs 2 and 3). The most informative first 600 ms after trial onset were included in the analysis, and sorted condition-wise (as for the GLM). Eye movement deviations in degrees of visual angle (from the midline) for each subject were entered into a session-wise 3 (condition: null/stay/shift) × 2 (direction of attention: left/right) repeated-measures ANOVA, and single conditions were compared using post hoc testing (Fisher's least significant difference).

Results

Task and Behavior

Three monkeys and 31 human subjects were trained and scanned with closely matched covert, selective, spatial-attention tasks that included interleaved periods of holding or shifting spatial attention. This task has proved itself instrumental in reliably localizing shift-selective human medial SPL (Vandenberghe et al. 2001; Molenberghs et al. 2007). Two pairs of peripherally presented shapes, each containing a behaviorally relevant and an irrelevant shape, were presented on the horizontal meridian (Fig. 1, top). Every 2250 ms, these stimuli were refreshed with no intervening time gap. Because subjects had learned to covertly track the relevant shapes, replacement of stimulus pairs could elicit either a spatial attention shift, when the relevant stimulus was replaced by the irrelevant stimulus of the second pair (shift event: Fig. 1-I,III), or allow attention to be maintained at the same location, when the relevant stimulus was replaced by the relevant member of the second pair (stay event: Fig. 1-II,V). To perform the task correctly, subjects were required to continuously fixate a central fixation point and to manually respond when the relevant stimulus dimmed (dim relevant, left attention: Fig. 1-IVa). Correct responses were followed by auditory (humans) or liquid reward (monkeys) feedback. Dimming of the irrelevant stimulus had to be ignored (dim irrelevant, left attention: Fig. 1-IVb). The task also included null events, in which the same stimuli were shown at the same location during 2 consecutive stimulus displays (null event: Fig. 1-VI). Hence, the subject kept his attention focused toward the same hemifield, while the visual display remained unchanged for 2 consecutive trials. Importantly, relevant and irrelevant dimming trials used to probe the allocation of attention were rare (14% of the trials), were equally present

in all conditions, and temporally dissociated (50–1500 ms) from the actual stay, shift, or null events.

Subjects almost never responded to dimmings of the irrelevant shapes, with a false alarm rate close to zero for humans (0.25% [SD 0.22]) and monkeys (M13 = 0.14% [SD 0.34)], M24 = 0.5% [SD 0.84], M35 = 0.06% [SD 0.19]). Furthermore, the eye trace within the fixation window tended to deviate slightly toward the direction of the relevant stimulus in both humans (Supplementary Fig. 2, repeated-measures (r) ANOVA with factors condition (3) × direction of attention (2); factor direction of attention (left vs. right): $F_{(1,21)} = 0.86$, $P = 0.36$, not significant) and monkeys (Supplementary Fig. 3, significant for M13, M24, but not for M35, 3 × 2 rANOVA, factor direction of attention (left vs. right): M13: $F_{(1,7)} = 5.9$; $P = 0.04$; M24: $F_{(1,11)} = 24.67$; $P = 0.0004$; M35: $F_{(1,9)} = 0.09$; $P = 0.78$). Note that the deviations in eye position were much smaller in monkeys compared with humans. This is partially due to the longer training of the monkeys which resulted in better fixation behavior. Another mutually nonexclusive explanation, however, is that the quality of the eye recordings inside the scanner is significantly better for our monkey compared with our human setup. We mainly suffer from the specifics of the phased array coil arrangement in the human setup which renders it difficult to obtain stable eye-movements during the entire duration of a human experiment.

RTs in humans were slightly longer immediately after shift compared with stay and null events (see Supplementary Table 1 "RT", rANOVA [condition (3) × direction of attention (2), factor direction of attention $F_{(2,60)} = 4.06$, $P = 0.02$]), exactly as previously reported (Molenberghs et al. 2007). However, no significant differences in RTs across conditions were observed in monkeys (Supplementary Table 2 "RT", M13: $F_{(2,14)} = 2.48$, $P = 0.11$; M24: $F_{(2,22)} = 0.051$, $P = 0.95$; M35: $F_{(2,18)} = 3.41$, $P = 0.06$). This might be due to the extensive training regime that our monkeys experienced prior to scanning. Neither monkeys nor humans showed significant differences in hits and misses between stay, shift, and null trials, indicating that they performed equally well across conditions (rANOVA, factor conditions: null, stay, shift, Supplementary Table 2 for monkeys, Supplementary Table 1 for humans, misses in humans for factor condition: $F_{(2,60)} = 0.57$, $P = 0.60$).

Shift-Activations in Humans and Monkeys: GLM

We first computed the contrast shift versus stay to identify shift regions in each species. Spatial attention shifts activated the human mSPL most strongly (Fig. 2A,C, Supplementary Table 3, and Supplementary Figs 4 and 5 for details), consistent with previous reports (Vandenberghe et al. 2001; Yantis et al. 2002; Molenberghs et al. 2007). In monkeys, the strongest activations for attention shifts were found bilaterally in medial occipito-parietal area V6A, left MIP and in area 46 and anterior cingulate cortex (ACC) in frontal cortex (see Fig. 2B,D; Supplementary Table 4, and Supplementary Figs 5 and 6 for more detail).

Interestingly, the strongest shift voxels of human medial SPL (Fig. 2C) abutted the known cytoarchitectonically defined regions SPL5 and SPL7 (Eickhoff et al. 2005; Scheperjans et al. 2008) at their occipital borders. Additional shift activations in humans (Fig. 2A,C) were located bilaterally in the medial frontal gyrus, the right superior frontal gyrus, and the inferior parietal lobule (IPL). In monkeys (Fig. 2B,D), corresponding activations were located bilaterally in areas 46, and temporal-parietal-occipital cortex (TPOC), caudo-medial occipital cortex (cmoc), ACC, lateral intraparietal area (LIP), medial F6 and right area 12. Whereas the shift activation in monkey IPL was located within bilateral TPOC (Mantini et al. 2011) (Fig. 2D, and Supplementary Fig. 5), the activation in human IPL corresponded to a location at the borders of cytoarchitectonically defined areas PGa and PFm (Caspers et al. 2006) (Fig. 2C). Based upon shift activations in monkeys (Fig. 2B,D, and Supplementary Fig. 5) revealed by the contrast shift versus stay, several frontal and parietal regions were previously labeled as "shift-selective" (Caspari et al. 2015). "Shift-selective" regions were defined as activated for bilateral spatial attention shifts, irrespective of the direction of the attention shift, according to the original definition of human shift-selective SPL (Yantis et al. 2002). In the monkey, these regions included areas V6/V6A, MIP, TPOC, somatomotor cortex, the anterior principal sulcus (anterior area 46), area F6, as well as the ACC, but not "cmoc" (Caspari et al. 2015). Due to its selectivity for the direction of attention, cmoc was excluded as a potential mSPL homolog. Using the ISBC analysis, we next attempted to identify, in a data-driven manner, which of the monkey shift regions best corresponded to human shift-selective mSPL.

ISBC Across Humans and Monkeys

By correlating the condition-specific "beta-fingerprints" of the human SPL region (and its sub-divisions) with condition-specific beta-fingerprints of (1) single voxels, and (2) also anatomical ROIs in monkeys, we proposed to determine functional correspondences between species that were devoid of any spatial assumptions. Beta-fingerprints for single ROIs or voxels were obtained by first computing a GLM across sessions (monkey) or subjects (human), thereby modeling the 10 task events defining the experimental paradigm: null left (example in Fig. 1, VI); null right; stay left (Fig. 1, V); stay right (Fig. 1, II); shift left (Fig. 1, III); shift right (Fig. 1, I); dim answer, left attention (Fig. 1, IVa); dim answer, right attention; dim no answer, left attention (Fig. 1, IVb); dim no answer, right attention. The combination of these 10 beta-values constituted the beta-fingerprint of a voxel or ROI. Next, we correlated the average beta-fingerprints of the shift-selective mSPL-cluster in our 31 human subjects with the beta-fingerprints obtained from each individual cortical voxel from all sessions acquired in the 3 monkey subjects. Furthermore, we also correlated the beta-fingerprints of distinct subdivisions of the human SPL region, 2 cytoarchitectonic (independent of shift-selectivities) and one functional subdivision, with anatomically pre-defined ROIs in monkeys. This approach allowed us to characterize the functional correspondences between sub-compartments of human SPL and their monkey counterparts without prior knowledge concerning task-related activations in the monkey.

Correlating Human Shift-Selective mSPL Beta-Fingerprints with Single Voxels in Monkey

Our first aim was to identify those voxels in monkey cortex that correlate with the beta-fingerprint of the shift-selective human mSPL-cluster as determined in the present and previous studies (Fig. 3A, top) (Vandenberghe et al. 2001; Yantis et al. 2002; Molenberghs et al. 2007; Chiu and Yantis 2009), without biasing ourselves to any specific pre-defined location or ROI in the monkey.

Besides the expected shift-selectivity (the property used to define the cluster), the average mSPL-cluster beta-values (human) also revealed a selectivity for the dim-no-answer conditions (bar-plot, Fig. 3A). These represent irrelevant dimming events (example in Fig.1, IVb) during which attention was allocated to a relevant stimulus, while an unexpected dimming of

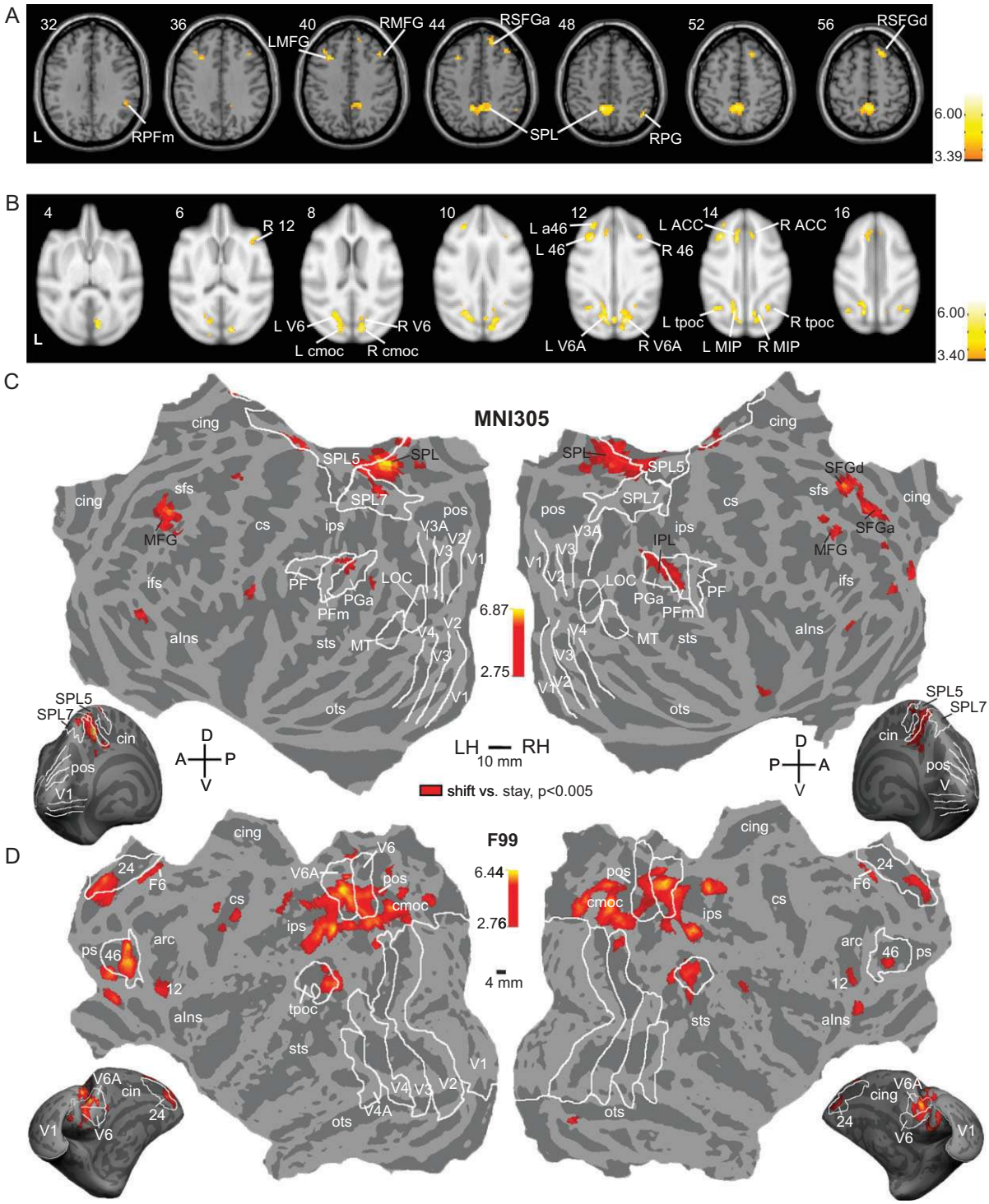

Figure 2. Shift activations in humans and monkeys (GLM-based). Contrasting shift (left and right) versus stay (left and right) in humans (*A*, *C*, random effects analysis) and in monkeys (*B*, *D*, mixed-effects analysis). Representation of shift activations in the brain volume (see Supplementary Figs 4 and 6 for coronal sections of humans/ monkeys) (*A*) for humans on the Colin-brain (MNI space), with respective ROI labels, local maxima and *t*-values of the activations are listed in Supplementary Table 3; (*B*) for monkeys on the RM112-in-F99 space template, respective local maxima and *t*-values of ROI-labels are listed in Supplementary Table 4. Shift activations displayed on the inflated F99 gray matter surface (LH, left hemisphere on the left; RH, right hemisphere on the right) with corresponding ROI labels (*C*) in humans on the inflated and flattened FreeSurfer fsaverage (MNI305) brain; anatomical labels displayed in black, ROI-labels indicated in white. V1–V3,V3A,V4, MT, LOC obtained from the PALS-B12 atlas (FreeSurfer); SPL5 and SPL7 (Scheperjans et al. 2008), PGa, PFm, and area PF (Caspers et al. 2006) and labels of anatomical locations were obtained from the SPM8 anatomy toolbox (Eickhoff et al. 2005). Abbreviations: MFG, medial frontal gyrus; SPL, superior parietal lobe; IPL, inferior parietal lobe; SFG, superior frontal gyrus; (*D*) in monkeys on the inflated and flattened F99 template. Origins of the monkey ROI-label are listed in Supplementary Table 6. (*C*,*D*) Bottom left and right: posterior-medial view of the inflated brain, exposing medial parietal cortex. Sulci: cing, cingulate; sfs, superior frontal; ifs, inferior frontal; ains, anterior insular; sts, superior temporal; cs, central; ips, intraparietal; pos, parieto-occipital; ots, occipito-temporal; ps, principal; arc, arcuate sulcus.

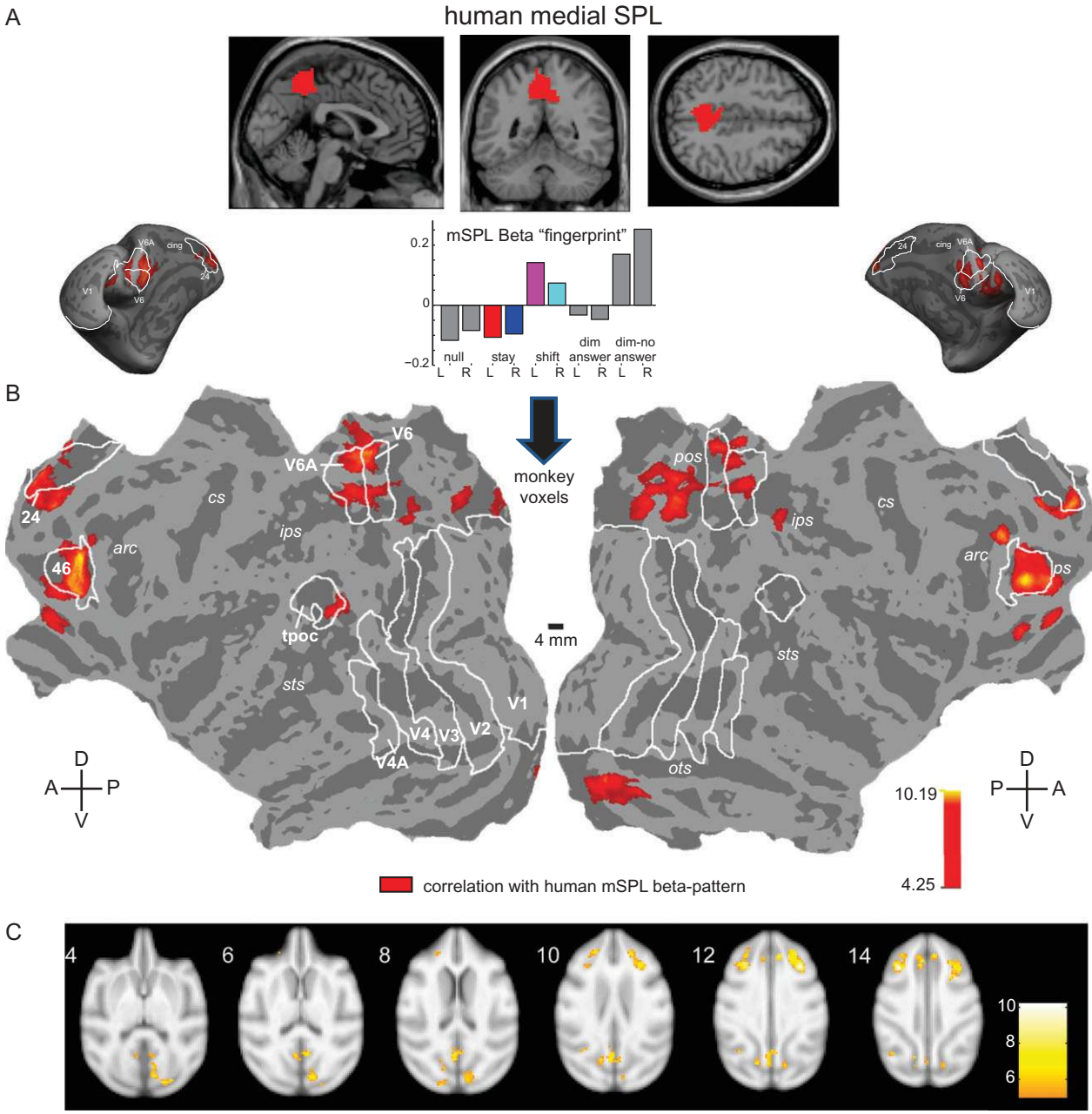

Figure 3. Correlation between the "beta-fingerprint" of the human shift-selective "mSPL" and all voxels in monkey. (*A*) 3-D sections (Colin-brain) exposing the medial shift-selective SPL-cluster ("mSPL") in human, as identified by contrasting bilateral shift with bilateral stay conditions. Bar plots represent the condition-specific beta-fingerprint across all voxels of this ROI, averaged across 31 human subjects. (*B*,*C*) Voxels in the monkey brain that correlate with the human "mSPL" beta-fingerprint, obtained from a session-wise mixed-effects (MFX) analysis across 30 sessions, collected in 3 monkey subjects, displayed (*B*) on the inflated and flattened gray matter surface (F99), and (*C*) in the RM112-in F99 template volume for transverse sections (from +4 to +14 centered on the anterior commissure). See Supplementary Table 5 for the list of activated ROIs, their coordinates and corresponding peak *t*-values.

the irrelevant stimulus occurred in the contralateral hemifield. In fact, the dimming of the irrelevant shapes represents a bottom-up-driven visual event which must have triggered a quick, transient, covert attention shift from the attended to the unattended hemifield. Hence, it is not surprising that the irrelevant dimmings led to even stronger beta-values in the shift-selective regions compared with the shift events, since they most likely evoked a double shift in attention. The mSPL beta-fingerprint (Fig. 3A, bar-plot) was correlated with the beta values (for the same 10 conditions) of each voxel of each session obtained separately in the 3 monkeys. A second-level analysis across sessions with the *z*-scored correlation maps, revealed significantly correlated voxels (Fig. 3B,C, Supplementary Fig. 1) in monkey caudo-parietal regions including areas V6/V6A (more so in V6A than V6) and in the right hemisphere some regions slightly more posteriorly (cmoc). In addition, significant correlations were found in the posterior end of the STS (left TPOC) and frontally in right FEF, bilateral area 46, area 24 (ACC) and left area 11 (see Fig. 3C, slice no.8; for a detailed list see Supplementary Table 5). In general, these ISBC maps corresponded surprisingly well with the GLM-based *t*-score maps (Fig. 2). The beta-fingerprints of the monkey areas that

correlated with human mSPL are shown in Supplementary Fig. 7. They show the expected shift selectivity, and also a pronounced difference between relevant and irrelevant dimming events, again indicating that the irrelevant dimmings most likely evoke a double shift in spatial attention.

Functional Heterogeneity of Human SPL Based on Shift-Selective Responses?

Finally, we attempted to assess how beta-fingerprints from subdivisions of human SPL might correlate with independently defined anatomical ROIs in monkeys (displayed in Supplementary Fig. 1, and Supplementary Table 6). Human SPL was subdivided into 2 known cytoarchitectonic ROIs SPL5 (Fig. 4A, red), and SPL7 (Fig. 4A, yellow) (Eickhoff et al. 2005; Scheperjans et al. 2008; Scheperjans et al. 2008), and a third ROI, consisting of those voxels within the medial SPL cluster showing the highest shift-selective beta-values (referred to as SPLmx, Fig. 4A, white crosses). To avoid overlap of the SPL-shift cluster with the cytoarchitectonic ROIs, SPLmx was defined as an aggregate of 3 mm radius spheres centered upon the 4 highest local maxima (surviving FWE-correction, $P = 0.05$) within the SPL-shift cluster (see Supplementary Table 3, SPL1-4). This approach was also useful to determine the monkey ROI to which the most shift-selective portion of human SPL corresponded. As previously indicated in Fig. 2C, and as shown here in the 3D volume (Fig. 4A), the medial shift-selective SPL-cluster was caudo-ventrally situated in the medial wall below the cytoarchitectonically defined areas SPL5 and SPL7.

Figure 4B displays the beta-fingerprints of the 3 human SPL-ROIs. Whereas SPL5 and SPLmx were more selective for shift than for stay conditions (2 × 2 repeated-measures ANOVA (rANOVA) with factors "condition" (shift, stay) and direction of attention (left/ right); factor condition: $F_{(1,30)} = 8.66$, $P = 0.006$), this was not the case for SPL 7 ($F_{(1,30)} = 0.04$, $P = 0.84$). SPL7 was characterized by much smaller beta values for null events than for dim-no-answer conditions (when subjects have to refrain from making a manual response) compared with all other conditions ($P < 0.011$, Fisher's least significant difference test; post hoc test after 5 (condition) × 2 (direction of attention) rANOVA). Overall, SPL7 was more responsive to bottom-up-driven, irrelevant dimmings relative to all other conditions ($P < 0.018$, Fisher's least significant difference test) and compared with SPL5 (2 (ROI: dim-no answer SPL5/ dim-no answer SPL5) × 2 (direction of attention: left/right) rANOVA, $F_{(1,30)} = 17.35$; $P = 0.0002$)). Next, the average beta-fingerprints of each monkey ROI were tested for correlation with the single-subject ($N = 31$) beta-fingerprints from the 3 human SPL-subdivisions (Fig. 4C). SPL5 was significantly correlated only with right monkey TPOC, whereas SPL7 correlated with right MT and right MSTv, but also with right TPOC, right V6, left V6Ad/v, and left area 31 (after correcting for multiple comparisons). SPLmx was most selectively correlated with medial parietal cortex ROIs V6 and V6A, and to right TPOC and left area 31. Although SPL7 was correlated with more regions outside of medial parietal cortex (compared with SPLmx), the correlation pattern of SPL7 resembled that of SPLmx (pairwise linear correlation coefficient $r = 0.86$, $P \ll 0.00001$), whereas that of SPL5 did not ($r = 0.03$, $P = 0.77$). Next, we further subdivided SPL5 and SPL7 into their known subdivisions (Scheperjans et al. 2008). Supplementary Fig. 8 shows the subdivisions of SPL5 and SPL7, Supplementary Fig. 9A the respective beta-fingerprints, and Supplementary Fig. 9B the correlations between these fingerprints and those of the monkey ROIs (as in Fig. 4). This additional analysis confirmed the virtual lack of correlations between the SPL5 subdivisions and the areas in the posterior parietal lobe of monkeys. In addition, the SPL7 subdivisions showed a more heterogenous pattern of correlations, with relatively high correlations between SPL 7a and 7pc with many monkey ROIs, including V6 and V6Ad/v. Close inspection of the respective beta-fingerprints of SPL 7a and 7pc, however, confirms the lack of shift-selectivity (2 × 2 rANOVA with factors condition (shift, stay) and direction of attention (left/ right); factor condition not significant for SPL 7a ($F_{(1,30)} = 0.62$; $P = 0.4326$) and SPL 7pc ($F_{(1,30)} = 0.03$; $P = 0.8541$), suggesting that the ISBCs may rather be driven by the difference between the relevant and irrelevant dimming events. Thus, although the ISBCs from the SPL subdivisions reveal interesting comparative information, they are less relevant with regard to the substrate subserving shift-selective responses in both species.

In general, based on the condition-wise selectivity profiles (beta-fingerprints) from SPLmx in combination with the spatial locations of shift-selective regions across analyses, our results indicate that monkey medial parietal cortex most consistently matched human shift-selective mSPL (Figs. 3B and 4C).

Discussion

We obtained consistent shift activations in parietal and frontal regions of humans and monkeys based on the contrast shift versus stay, independently of the direction of the shifts. The strongest shift signals were found in human medial SPL and caudo-medial parietal cortex in monkeys (Fig. 2). In addition, we observed a strong signal during bottom-up-driven irrelevant dimmings in mSPL. This signal is not unexpected, as irrelevant dimming events most likely trigger transient shifts in attention.

Correlations between the task-related beta-values of human mSPL with those of individual voxels in the monkey (ISBC method) showed that in monkeys, medial parietal cortex and regions including area 46, ACC, right FEF, right cmoc, and left TPOC, were involved in task-based computations similar to those of the human mSPL-cluster (Fig. 3B). Hence, this spatially unbiased, voxel-wise correlation approach has largely confirmed the GLM-results (Fig. 2). Using the ROI-wise ISBC method, we showed that the part of human medial SPL showing the greatest degree of shift-selectivity (SPLmx, Fig. 4) correlated best with monkey areas V6 and V6A, in addition to right TPOC and left area 31. Thus, task-based correlations with human shift-selective SPL (SPLmx, Fig. 4) were most abundant in areas of medial posterior parietal cortex in the monkey.

By applying the ISBC method, we could ascertain finer-grained correspondences across species. Indeed, ISBC takes advantage of the entire set of modeled conditions, rather than limiting the conditions to those entering the GLM-contrast used to define shift-sensitivity (shift left/right vs. stay left/right). In general, this novel analytical method is quite appealing, since it can be used to establish task-based functional correspondences across species, considering all modeled conditions, even when they occur in temporally dissimilar orders across species and experiments. This is a huge advantage relative to comparative approaches based on GLM contrasts only and also compared with our previous comparative ISAC tool (Mantini et al. 2012), whereby the timings of the task or sensory stimulation events need to be perfectly synchronized in the 2 species.

Subdivisions of the SPL

Multiple functional properties have been attributed to the superior parietal lobule in both species. A gradient from visual processing in posterior SPL to stronger somatosensory influences

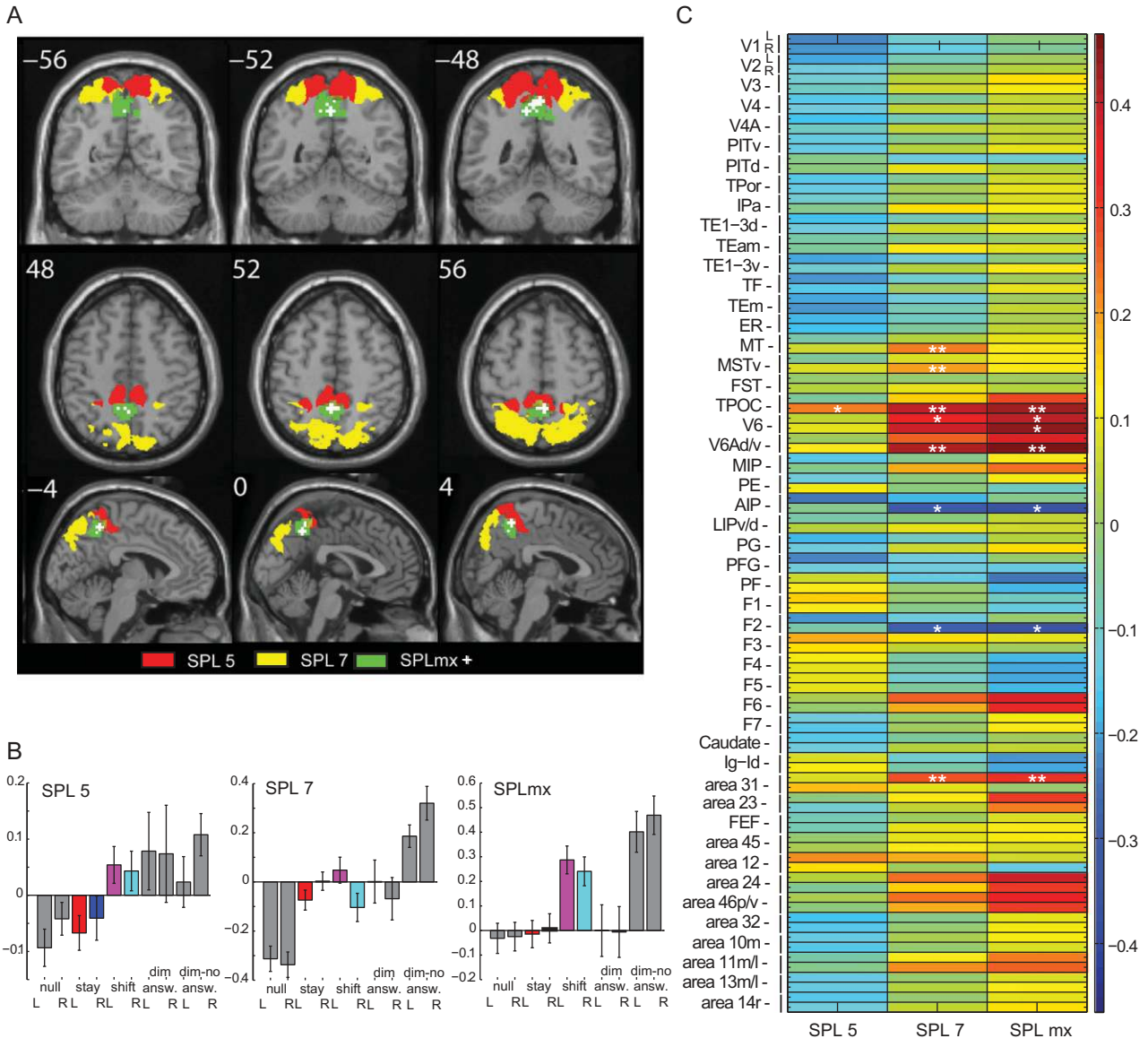

Figure 4. Beta-correlations of monkey anatomical ROIs with subdivisions of the human SPL. (*A*) Volume-slices through the human brain (Colin-brain, MNI space, coronal/ transverse/ sagittal sections), displaying the locations of 2 anatomically defined ROIs (Eickhoff et al. 2005) (SPL5, red; SPL7, yellow), and the functionally defined shift-selective medial SPL-cluster (green), including its 4 highest local maxima (white crosses). (*B*) Beta-fingerprints of SPL5, SPL7, and SPLmx, averaged across 31 subjects; Error bars denote the standard error of the mean across subjects. (*C*) Cross-correlation matrix of the human SPL beta-fingerprints with the average monkey beta-fingerprints of independently defined anatomical ROIs (listed in Supplementary Table 6, and displayed in Supplementary Fig. 1). The average beta-value (across all sessions of all monkeys) was calculated for each monkey ROI and correlated with the SPL-ROIs across single human subjects. Significances were computed based on random-effects statistics across human subjects and the resulting correlation matrices were Bonferroni-corrected for the number of comparisons indicated at $^{*}P < 0.05$, and $^{**}P < 0.01$ (98 monkey ROIs × 3 human SPL-ROIs). Abbreviations: ER, entorhinal cortex; TPOC, temporo-parietal occipital cortex; MIP, medial intraparietal area; AIP, anterior intraparietal area; LIP, lateral intraparietal area; Ig-Id, insular cortex (g, granular; d, dysgranular); FEF, frontal eye fields; v, ventral; d, dorsal; m, medial; l, lateral; r, rostral.

in anterior SPL has been reported (Squatrito et al. 2001; Stoeckel et al. 2004; Breveglieri et al. 2006; Wenderoth et al. 2006; Wang et al. 2015). This caudo-rostral functional gradient is also reflected in the cytoarchitectonic organization of SPL (i.e. the neurotransmitter receptor distribution) (Scheperjans et al. 2008), whereby posterior portions in SPL 7 resembled the patterns seen in visual areas (see also Gillebert et al., 2013), while more anterior regions in SPL 5 displayed patterns similar to somatosensory cortex (Scheperjans et al. 2005). A similar functional gradient exists within monkey areas V6/V6A itself, where V6A belongs to classical visual-association cortex (Gamberini et al. 2015). Cells in the ventral part of the anterior bank of the parieto-occipital sulcus (area V6 more than V6Av) are very sensitive to visual stimulation (Galletti et al. 1991), whereas cells located more dorsally (V6Ad more than V6Av) are more sensitive to somatosensory stimulation (Gamberini et al. 2011), with an increasing somatosensory influence in the more dorsally located area, PEc (Breveglieri et al. 2008).

The pattern of beta-values in posteriorly located SPL7 (Fig. 4B) corroborated the visual nature of that region. Indeed, SPL7 responded most strongly to bottom-up driven irrelevant dimmings above all other conditions. Negative beta values

were even observed in SPL7 for null events, during which visual stimulation did not change. This region also showed correlated beta-series with visual areas MT and MSTv in monkeys, as opposed to SPL5 and SPLmx (Fig. 4C). The correlation matrix of SPL7 was more similar to SPLmx than SPL5, as the former 2 regions were significantly correlated with left area V6, right V6Ad/v, and left area 31 of the monkey. These correlations are mostly driven by the strong selectivity for the dim-no-answer condition. Top-down-directed shift-selectivity (see shift-conditions in Fig. 4B), however, was present in SPL5 but not SPL7. Intriguingly, the strongest shift-selective cluster (SPLmx) within the medial superior parietal lobule also responded to bottom-up-generated, unexpected irrelevant dimmings (Fig. 4B, rightmost, dim-no-answer conditions). Hence, this region, located ventro-medially to SPL5 and antero-medially to SPL7 which may correspond to the visual medial parietal subdivision as described by Margulies et al. (2009), appears to give rise to a unique signal to shift, that is independent of somatosensory or motor components. In conclusion, human SPL can be subdivided, based not only on its cytoarchitecture (Eickhoff et al. 2005; Scheperjans et al. 2005; Scheperjans et al. 2008; Scheperjans et al. 2008) and task-based activation profiles (Vandenberghe et al. 2001; Yantis et al. 2002; Grefkes et al. 2004), but also with respect to its functional correspondences with monkey SPL.

Function and Connections of Areas V6 and V6A in Monkey Compared with Human SPL

Function

The human medial SPL and monkey V6A are both regions located within the dorso-medial visual stream (Rizzolatti and Matelli 2003; Fattori et al. 2015), processing visual information to guide actions (Milner and Goodale 2008). Area V6A in monkey is a crucial node of the dorso-medial visual stream, at the origin of several pathways for visuo-spatial processing (Galletti et al. 2003; Rizzolatti and Matelli 2003), located at the most anterior bank of the parieto-occiptial sulcus. V6A contains neurons exhibiting attention, saccade, reach, and grasping-related activity (Galletti et al. 1996, 1999, 2010; Kutz et al. 2003; Fattori et al. 2004, 2005; Premereur et al. 2015), so it is not a pure visual area as imprecisely suggested by its name. Similar functions can be attributed to a cluster of regions in human mSPL, as revealed with fMRI during 4 different visuo-spatial tasks (Simon et al. 2002): covert shifts of attention, voluntary saccades, and spatially specific grasping and pointing. Two recent repetitive TMS studies demonstrated interference with spatial-attention shifts upon stimulation of human mSPL, with one of these studies (Capotosto et al. 2013) targeting locations corresponding to the shift-selective region as defined in the current and previous studies (Yantis et al. 2002; Molenberghs et al. 2007; Shulman et al. 2009). The TMS studies revealed a selective impairment during covert spatial attention shifts, but not during contralateral orienting (Capotosto et al. 2013). In the second study, rTMS was applied over the dorsal-most part of the anterior bank of the POS ("SPOC") (Ciavarro et al. 2013), which is located slightly more postero-ventrally relative to shift-selective mSPL and which most likely corresponds to human area V6A. The authors interfered with attentional "re-orienting" during a reaching and an attention task, where they found an effect during the invalidly- but not the validly-cued trials. One possible interpretation might be that both functions—covert shifts of attention and reorienting of attention for an immediate reaching movement—are coded in distinct portions of the human parietal cortex (mSPL for abstract spatial shifts, and SPOC for reorienting and reaching movements), which are anatomically integrated within the V6/V6A complex of monkeys. Importantly, we have shown here that the shift-selective activations in the V6/V6A complex occurs independently of the motor events, which were temporally disconnected from the shift events and equiprobable during the shift and stay conditions.

Anatomy and Connections

Within the superior parietal lobule of the monkey, shift selectivity was found in areas V6, V6A and some more posteriorly located regions. The human shift-selective mSPL region, on the other hand, is located on the mesial surface of the hemisphere and does not correspond to human areas V6, V6Av, and V6Ad, which are located near the top of the parieto-occipital sulcus (Pitzalis et al. 2006; Pitzalis et al. 2013; Pitzalis et al. 2015; Tosoni et al. 2015). This surprising finding corroborates earlier evidence (Mantini et al. 2012), that putative "homologous" areas, as based on their position and similarities in retinotopic and functional properties, may share some but not all functions. Although it is impossible to obtain conclusive evidence because we have no access to the common ancestors of humans and macaques, this suggests that some functions may have shifted from one area in that ancestor to different neighboring regions in currently living species of that ancestor. Other properties, such as the retinotopic organization may have been conserved. The implication is that regions can only be considered "partially homologous" and that under evolutionary pressure some properties originally residing in the same region may have been pushed to other regions, for instance to enable the emergence of novel species-specific properties in such areas. Alternatively, attention shifting is a property that evolved entirely independent in humans and macaques in different neural substrates. We think, however, that the latter scenario is less likely since the strongest attentional-shift activity within the parietal lobe is found in relatively similar topological regions in both species.

Via its direct anatomical connections with the more ventrally located visual area V6, which is connected to visual areas V1, V2/V3/V3A, V4t and MT (Galletti et al. 2001), area V6A receives dorsal-stream information (Gamberini et al. 2009; Passarelli et al. 2011). Besides prominent parietal projections from MIP and weaker projections from LIP and medial cingulate areas 23 and 31, V6A also receives frontal lobe projections from area 46, FEF, and area F7 (Passarelli et al. 2011). Consistent with this anatomical connectivity pattern, many of the latter areas showed shift-selectivity (Figs 2–4). This also explains why beta-fingerprints of human mSPL are strongly correlated with V6/V6A itself, in addition to regions that are anatomically connected to the latter. Furthermore, V6A also receives higher order visual and somatic input from the lateral posterior and medial pulvinar nuclei (Gamberini et al. 2015). Monkey V6A is thus positioned where object and spatial information can be integrated for rapid activation of circuits involved in attention and spatially guided actions (Rosa et al. 2009). Our selective attention task shows that the visuo-spatial component, measured here via spatial attention shifts, appears to be a strong driver of the V6/V6A complex, in the absence of motor action. This is also the case for human shift-selective mSPL, as it most consistently matched the functional properties of areas V6/V6A.

Corresponding Evidence from Lesion Studies

Patient lesion studies involving SPL and an inactivation study of monkey V6A provides corroborating evidence that these regions may be, at least partially, functionally homologous.

Bilateral superior parietal lesions in humans have previously been associated with Balint syndrome (Bálint 1909; Damasio et al. 2000), resulting in an erratic fixation pattern (Damasio et al. 2000), impaired control of intentional eye movements, and spatial errors in visually guided arm movements and reaching (Ptak and Müri 2013). Other human lesion studies have confirmed the role of SPL in shifting spatial attention during invalidly-cued trials (Vandenberghe et al. 2012) and during the detection of a displaced visual and auditory stimulus (Phan et al. 2000). Similarly a lesion study of area V6A in green monkeys yielded deficits in reaching, wrist orientation, and grasping (Battaglini et al. 2002). Unfortunately, eye movements were not recorded in this study, leaving unaddressed whether the observed motor deficits were caused by impaired eye-movement patterns or disrupted by attentional shifts in general. The results of these lesion studies and those of the present experiment, whereby spatial attention shifts were temporally dissociated from the actual motor output, argue in favor of the hypothesis that the observed lesion symptoms may underlie a common disturbance in mechanisms necessary to compute spatial attention shifts, rather than being linked to specific motor outputs (Vandenberghe et al. 2001, 2012). Thus, in addition to the similarities in the functional and anatomical connectivity profiles of human mSPL and monkey V6A, lesion data adds to the evidence that they are both involved in the control of a fast transformation of spatial coordinates even in the absence of overt behavior (Vandenberghe et al. 2001; Molenberghs et al. 2007).

Conclusion

Using a covert spatial attention task, novel analytical techniques and known anatomical-tract tracing data in monkeys, we obtained further evidence for functional correspondences between human mSPL and monkey areas V6A. In general, the current findings stress the importance and validity of the monkey model for studying fundamental cognitive processes. Furthermore, the novel ISBC approach can become an exquisite tool to determine, in an entirely data-driven manner, functional correspondences across species in general, as shown here for the superior parietal lobe. The current study also pointed to regions outside the superior parietal lobule showing functional similarities between monkeys and humans, which will be the focus of a future publication comparing attention processing in both species at a more general level.

Supplementary Material

Supplementary material is available at *Cerebral Cortex* online.

Funding

Inter-University Attraction Pole 7/11 to W.V. and R.V., the Research Foundation Flanders (senior clinical investigator grant and “G0660.09, G0A09.13” to R.V, and “G083111.10, G0A5613, G.062208.10, G0B8617, and Odysseus G0007.12” to W.V.); KU Leuven (OT/12/097) to R.V. and Programme Financing PFV/10/008 to R.V and W.V.; European Union Seventh Framework under grant agreement no. 604102 (Human Brain Project) to W.V., and Hercules to W.V and R.V.

Notes

The authors thank A. Coeman, C. Fransen, P. Kayenbergh, I. Puttemans, S. De Pril, A. Hermans, G. Meulemans, W. Depuydt, and M. Depaep for technical and administrative support and S. Raiguel for his comments on the manuscript. *Conflict of Interest*: None declared.

References

Arcaro MJ, McMains SA, Singer BD, Kastner S. 2009. Retinotopic organization of human ventral visual cortex. J Neurosci. 29:10638–10652.

Bálint DR. 1909. Seelenlähmung des “Schauens”, optische Ataxie, räumliche Störung der Aufmerksamkeit. Eur Neurol. 25:51–66.

Battaglini PP, Muzur A, Galletti C, Skrap M, Brovelli A, Fattori P. 2002. Effects of lesions to area V6A in monkeys. Exp Brain Res. 144:419–422.

Breveglieri R, Galletti C, Gamberini M, Passarelli L, Fattori P. 2006. Somatosensory cells in area PEc of macaque posterior parietal cortex. J Neurosci. 26:3679–3684.

Breveglieri R, Galletti C, Monaco S, Fattori P. 2008. Visual, somatosensory, and bimodal activities in the macaque parietal area PEc. Cereb Cortex. 18:806–816.

Capotosto P, Tosoni A, Spadone S, Sestieri C, Perrucci MG, Romani GL, Della Penna S, Corbetta M. 2013. Anatomical segregation of visual selection mechanisms in human parietal cortex. J Neurosci. 33:6225–6229.

Caspari N, Janssens T, Mantini D, Vandenberghe R, Vanduffel W. 2015. Covert shifts of spatial attention in the Macaque monkey. J Neurosci. 35:7695–7714.

Caspers S, Geyer S, Schleicher A, Mohlberg H, Amunts K, Zilles K. 2006. The human inferior parietal cortex: cytoarchitectonic parcellation and interindividual variability. Neuroimage. 33:430–448.

Chiu YC, Yantis S. 2009. A domain-independent source of cognitive control for task sets: shifting spatial attention and switching categorization rules. J Neurosci. 29:3930–3938.

Ciavarro M, Ambrosini E, Tosoni A, Committeri G, Fattori P, Galletti C. 2013. rTMS of medial parieto-occipital cortex interferes with attentional reorienting during attention and reaching tasks. J Cogn Neurosci. 25:1453–1462.

Damasio AR, Tranel D, Rizzo M. 2000. Disorders of complex visual processing. In: Mesulam MM, editor. Principles of behavioral and cognitive neurology. New York: Oxford University Press. p. 332–372.

Eickhoff SB, Stephan KE, Mohlberg H, Grefkes C, Fink GR, Amunts K, Zilles K. 2005. A new SPM toolbox for combining probabilistic cytoarchitectonic maps and functional imaging data. Neuroimage. 25:1325–1335.

Ekstrom LB, Roelfsema PR, Arsenault JT, Kolster H, Vanduffel W. 2009. Modulation of the contrast response function by electrical microstimulation of the macaque frontal eye field. J Neurosci. 29:10683–10694.

Fattori P, Breveglieri R, Amoroso K, Galletti C. 2004. Evidence for both reaching and grasping activity in the medial parieto-occipital cortex of the macaque. Eur J Neurosci. 20:2457–2466.

Fattori P, Breveglieri R, Bosco A, Gamberini M, Galletti C. 2015. Vision for prehension in the medial parietal cortex. Cereb Cortex. 27:1149–1163.

Fattori P, Breveglieri R, Marzocchi N, Filippini D, Bosco A, Galletti C. 2009. Hand orientation during reach-to-grasp movements modulates neuronal activity in the medial posterior parietal area V6A. J Neurosci. 29:1928–1936.

Fattori P, Kutz DF, Breveglieri R, Marzocchi N, Galletti C. 2005. Spatial tuning of reaching activity in the medial parieto-occipital cortex (area V6A) of macaque monkey. Eur J Neurosci. 22:956–972.

Ferry AT, Öngür D, An X, Price JL. 2000. Prefrontal cortical projections to the striatum in macaque monkeys: Evidence for an organization related to prefrontal networks. J Comp Neurol. 425:447–470.

Friston KJ, Stephan KE, Lund TE, Morcom A, Kiebel S. 2005. Mixed-effects and fMRI studies. Neuroimage. 24:244–252.

Galletti C, Battaglini PP, Fattori P. 1991. Functional properties of neurons in the anterior bank of the parieto-occipital sulcus of the Macaque monkey. Eur J Neurosci. 3:452–461.

Galletti C, Breveglieri R, Lappe M, Bosco A, Ciavarro M, Fattori P. 2010. Covert shift of attention modulates the ongoing neural activity in a reaching area of the macaque dorsomedial visual stream. PLoS One. 5:e15078.

Galletti C, Fattori P, Battaglini PP, Shipp S, Zeki S. 1996. Functional demarcation of a border between areas V6 and V6A in the superior parietal gyrus of the macaque monkey. Eur J Neurosci. 8:30–52.

Galletti C, Fattori P, Gamberini M, Kutz DF. 1999. The cortical visual area V6: brain location and visual topography. Eur J Neurosci. 11:3922–3936.

Galletti C, Gamberini M, Kutz DF, Fattori P, Luppino G, Matelli M. 2001. The cortical connections of area V6: an occipito-parietal network processing visual information. Eur J Neurosci. 13: 1572–1588.

Galletti C, Kutz DF, Gamberini M, Breveglieri R, Fattori P. 2003. Role of the medial parieto-occipital cortex in the control of reaching and grasping movements. Exp Brain Res. 153: 158–170.

Gamberini M, Bakola S, Passarelli L, Burman KJ, Rosa MG, Fattori P, Galletti C. 2016. Thalamic projections to visual and visuomotor areas (V6 and V6A) in the Rostral Bank of the parieto-occipital sulcus of the Macaque. Brain Struct Funct. 221:1573–1589.

Gamberini M, Fattori P, Galletti C. 2015. The medial parietal occipital areas in the macaque monkey. Vis Neurosci. 32:E013.

Gamberini M, Galletti C, Bosco A, Breveglieri R, Fattori P. 2011. Is the medial posterior parietal area V6A a single functional area? J Neurosci. 31:5145–5157.

Gamberini M, Passarelli L, Fattori P, Zucchelli M, Bakola S, Luppino G, Galletti C. 2009. Cortical connections of the visuomotor parietooccipital area V6Ad of the macaque monkey. J Comp Neurol. 513:622–642.

Gillebert CR, Mantini D, Peeters R, Dupont P, Vandenberghe R. 2013. Cytoarchitectonic mapping of attentional selection and reorienting in parietal cortex. Neuroimage. 67:257–272.

Grefkes C, Ritzl A, Zilles K, Fink GR. 2004. Human medial intraparietal cortex subserves visuomotor coordinate transformation. Neuroimage. 23:1494–1506.

Holmes AP, Friston KJ. 1998. Generalizability, random effects, and population inference. Neuroimage. 7:S34.

Janssens T, Keil B, Farivar R, McNab JA, Polimeni JR, Gerits A, Arsenault JT, Wald LL, Vanduffel W. 2012. An implanted 8-channel array coil for high-resolution macaque MRI at 3 T. Neuroimage. 62:1529–1536.

Janssens T, Zhu Q, Popivanov ID, Vanduffel W. 2014. Probabilistic and single-subject retinotopic maps reveal the topographic organization of face patches in the Macaque cortex. J Neurosci. 34:10156–10167.

Kelley TA, Serences JT, Giesbrecht B, Yantis S. 2008. Cortical mechanisms for shifting and holding visuospatial attention. Cereb Cortex. 18:114–125.

Kolster H, Mandeville JB, Arsenault JT, Ekstrom LB, Wald LL, Vanduffel W. 2009. Visual field map clusters in Macaque extrastriate visual cortex. J Neurosci. 29:7031–7039.

Kutz DF, Fattori P, Gamberini M, Breveglieri R, Galletti C. 2003. Early- and late-responding cells to saccadic eye movements in the cortical area V6A of macaque monkey. Exp Brain Res. 149:83–95.

Lewis JW, Van Essen DC. 2000a. Corticocortical connections of visual, sensorimotor, and multimodal processing areas in the parietal lobe of the macaque monkey. J Comp Neurol. 428:112–137.

Lewis JW, Van Essen DC. 2000b. Mapping of architectonic subdivisions in the macaque monkey, with emphasis on parieto-occipital cortex. J Comp Neurol. 428:79–111.

Madore B, Glover GH, Pelc NJ. 1999. Unaliasing by Fourier-encoding the overlaps using the temporal dimension (UNFOLD), applied to cardiac imaging and fMRI. Magn Reson Med. 42:813–828.

Mandeville JB, Marota JJA. 1999. Vascular filters of functional MRI: spatial localization using BOLD and CBV contrast. Magn Reson Med. 42:591–598.

Mantini D, Gerits A, Nelissen K, Durand JB, Joly O, Simone L, Sawamura H, Wardak C, Orban GA, Buckner RL, et al. 2011. Default mode of brain function in monkeys. J Neurosci. 31: 12954–12962.

Mantini D, Hasson U, Betti V, Perrucci MG, Romani GL, Corbetta M, Orban GA, Vanduffel W. 2012. Interspecies activity correlations reveal functional correspondence between monkey and human brain areas. Nat Methods. 9:277–282.

Margulies DS, Vincent JL, Kelly C, Lohmann G, Uddin LQ, Biswal BB, Villringer A, Castellanos FX, Milham MP, Petrides M. 2009. Precuneus shares intrinsic functional architecture in humans and monkeys. Proc Natl Acad Sci USA. 106:20069–20074.

McLaren DG, Kosmatka KJ, Oakes TR, Kroenke CD, Kohama SG, Matochik JA, Ingram DK, Johnson SC. 2009. A population-average MRI-based atlas collection of the rhesus macaque. Neuroimage. 45:52–59.

Milner AD, Goodale MA. 2008. Two visual systems re-viewed. Neuropsychologia. 46:774–785.

Molenberghs P, Mesulam MM, Peeters R, Vandenberghe R. 2007. Remapping attentional priorities: differential contribution of superior parietal lobule and intraparietal sulcus. Cereb Cortex. 17:2703–2712.

Nelissen K, Borra E, Gerbella M, Rozzi S, Luppino G, Vanduffel W, Rizzolatti G, Orban GA. 2011. Action observation circuits in the macaque monkey cortex. J Neurosci. 31:3743–3756.

Nelissen K, Luppino G, Vanduffel W, Rizzolatti G, Orban GA. 2005. Observing others: multiple action representation in the frontal lobe. Science. 310:332–336.

Neubert FX, Mars RB, Sallet J, Rushworth MF. 2015. Connectivity reveals relationship of brain areas for reward-guided learning and decision making in human and monkey frontal cortex. Proc Natl Acad Sci USA. 112:E2695–E2704.

Passarelli L, Rosa MG, Gamberini M, Bakola S, Burman KJ, Fattori P, Galletti C. 2011. Cortical connections of area V6Av in the macaque: a visual-input node to the eye/hand coordination system. J Neurosci. 31:1790–1801.

Phan ML, Schendel KL, Recanzone GH, Robertson LC. 2000. Auditory and visual spatial localization deficits following bilateral parietal lobe lesions in a patient with Balint's syndrome. J Cogn Neurosci. 12:583–600.

Pitzalis S, Bozzacchi C, Bultrini A, Fattori P, Galletti C, Di Russo F. 2013. Parallel motion signals to the medial and lateral motion areas V6 and MT+. Neuroimage. 67:89–100.

Pitzalis S, Fattori P, Galletti C. 2015. The human cortical areas V6 and V6A. Vis Neurosci. 32:E007.

Pitzalis S, Galletti C, Huang RS, Patria F, Committeri G, Galati G, Fattori P, Sereno MI. 2006. Wide-field retinotopy defines human cortical visual area v6. J Neurosci. 26:7962–7973.

Premereur E, Janssen P, Vanduffel W. 2015. Effector specificity in Macaque frontal and parietal cortex. J Neurosci. 35:3446–3459.

Pruessmann KP, Weiger M, Scheidegger MB, Boesiger P. 1999. SENSE: sensitivity encoding for fast MRI. Magn Reson Med. 42:952–962.

Ptak R, Müri R. 2013. The parietal cortex and saccade planning: lessons from human lesion studies. Front Hum Neurosci. 7:254.

Rissman J, Gazzaley A, D'Esposito M. 2004. Measuring functional connectivity during distinct stages of a cognitive task. Neuroimage. 23:752–763.

Rizzolatti G, Matelli M. 2003. Two different streams form the dorsal visual system: anatomy and functions. Exp Brain Res. 153:146–157.

Rosa MG, Palmer SM, Gamberini M, Burman KJ, Yu HH, Reser DH, Bourne JA, Tweedale R, Galletti C. 2009. Connections of the dorsomedial visual area: pathways for early integration of dorsal and ventral streams in extrastriate cortex. J Neurosci. 29:4548–4563.

Scheperjans F, Eickhoff SB, Homke L, Mohlberg H, Hermann K, Amunts K, Zilles K. 2008. Probabilistic maps, morphometry, and variability of cytoarchitectonic areas in the human superior parietal cortex. Cereb Cortex. 18:2141–2157.

Scheperjans F, Grefkes C, Palomero-Gallagher N, Schleicher A, Zilles K. 2005. Subdivisions of human parietal area 5 revealed by quantitative receptor autoradiography: a parietal region between motor, somatosensory, and cingulate cortical areas. Neuroimage. 25:975–992.

Scheperjans F, Hermann K, Eickhoff SB, Amunts K, Schleicher A, Zilles K. 2008. Observer-independent cytoarchitectonic mapping of the human superior parietal cortex. Cereb Cortex. 18:846–867.

Scheperjans F, Palomero-Gallagher N, Grefkes C, Schleicher A, Zilles K. 2005. Transmitter receptors reveal segregation of cortical areas in the human superior parietal cortex: relations to visual and somatosensory regions. Neuroimage. 28:362–379.

Shulman GL, Astafiev SV, Franke D, Pope DLW, Snyder AZ, McAvoy MP, Corbetta M. 2009. Interaction of stimulus-driven reorienting and expectation in ventral and dorsal frontoparietal and basal ganglia-cortical networks. J Neurosci. 29:4392–4407.

Simon O, Mangin JF, Cohen L, Le Bihan D, Dehaene S. 2002. Topographical layout of hand, eye, calculation, and language-related areas in the human parietal lobe. Neuron. 33:475–487.

Squatrito S, Raffi M, Maioli MG, Battaglia-Mayer A. 2001. Visual motion responses of neurons in the caudal area PE of Macaque monkeys. J Neurosci. 21:RC130–RC130.

Stoeckel MC, Weder B, Binkofski F, Choi HJ, Amunts K, Pieperhoff P, Shah NJ, Seitz RJ. 2004. Left and right superior parietal lobule in tactile object discrimination. Eur J Neurosci. 19:1067–1072.

Tosoni A, Pitzalis S, Committeri G, Fattori P, Galletti C, Galati G. 2015. Resting-state connectivity and functional specialization in human medial parieto-occipital cortex. Brain Struct Funct. 220:3307–3321.

Van Essen DC. 2004. Surface-based approaches to spatial localization and registration in primate cerebral cortex. Neuroimage. 23(Suppl 1):S97–S107.

Van Essen DC, Drury HA, Dickson J, Harwell J, Hanlon D, Anderson CH. 2001. An integrated software suite for surface-based analyses of cerebral cortex. J Am Med Inform Assoc. 8:443–459.

Vandenberghe R, Gitelman DR, Parrish TB, Mesulam MM. 2001. Functional specificity of superior parietal mediation of spatial shifting. Neuroimage. 14:661–673.

Vandenberghe R, Molenberghs P, Gillebert CR. 2012. Spatial attention deficits in humans: the critical role of superior compared to inferior parietal lesions. Neuropsychologia. 50: 1092–1103.

Vanduffel W, Fize D, Mandeville JB, Nelissen K, Van Hecke P, Rosen BR, Tootell RBH, Orban GA. 2001. Visual motion processing investigated using contrast agent-enhanced fMRI in awake behaving monkeys. Neuron. 32:565–577.

Wang L, Mruczek REB, Arcaro MJ, Kastner S. 2015. Probabilistic maps of visual topography in human cortex. Cereb Cortex. 25:3911–3931.

Wenderoth N, Toni I, Bedeleem S, Debaere F, Swinnen SP. 2006. Information processing in human parieto-frontal circuits during goal-directed bimanual movements. Neuroimage. 31:264–278.

Yantis S, Schwarzbach J, Serences JT, Carlson RL, Steinmetz MA, Pekar JJ, Courtney SM. 2002. Transient neural activity in human parietal cortex during spatial attention shifts. Nat Neurosci. 5:995–1002.

Zar JH. 1996. Biostatistical Analysis. Upper Saddle River, NJ: Prentice-Hall.